15. Zhu, X. K., O'Nions, R. K., Guo, Y. & Reynolds, B. C. Secular variation of iron isotopes in North Atlantic deep water. *Science* **287,** 2000–2002 (2000).
16. Belshaw, N. S., Zhu, X. K., Guo, Y. & O'Nions, R. K. High precision measurement of iron isotopes by plasma source mass spectrometry. *Int. J. Mass. Spectrom.* **197,** 191–195 (2000).
17. Marechal, C. N., Telouk, P. & Albarède, F. Precise analysis of copper and zinc isotopic compositions by plasma-source mass spectrometry. *Chem. Geol.* **156,** 251–273 (1999).
18. Clayton, R. N. & Mayeda, T. K. Formation of ureilites by nebular processes. *Geochim. Cosmochim. Acta* **52,** 1313–1318 (1988).
19. Clayton, R. N. & Mayeda, T. K. Oxygen isotope studies of achondrites. *Geochim. Cosmochim. Acta* **60,** 1999–2017 (1996).
20. Clayton, R. N. Mayeda, T. K., Goswami, J. N. & Olsen, E. J. Oxygen isotope studies of ordinary chondrites. *Geochim. Cosmochim. Acta* **55,** 2317–2337 (1991).
21. Volkening, J. & Papanastassiou, D. A. Iron isotope anomaly. *Astrophys. J.* **347,** L43–L46 (1989).
22. Volkening, J. & Papanastassiou, D. A. Zinc isotope anomaly. *Astrophys. J.* **358,** L29–L32 (1990).
23. Birck, J. L. & Lugmair, G. W. Nickel and chromium isotopes in Allende inclusions. *Earth Planet. Sci. Lett.* **90,** 131–143 (1988).
24. Rotaru, M., Birck, J. L. & Allègre, C. J. Clue to early solar system history from chromium isotopes in carbonaceous chondrites. *Nature* **358,** 465–470 (1992).
25. Podosek, F. A. *et al.* Thoroughly anomalous chromium in Orgueil. *Meteorit. Planet. Sci.* **32,** 617–627 (1997).
26. Niemeyer, S. & Lugmair, G. W. Titanium isotopic anomalies in meteorites. *Geochim. Cosmochim. Acta* **48,** 1401–1416 (1984).
27. Niemeyer, S. & Lugmair, G. W. Ubiquitous isotopic anomalies in Ti from normal Allende inclusions. *Earth Planet. Sci. Lett.* **53,** 211–225 (1981).
28. Papanastassiou, D. A. Chromium isotopic anomalies in the Allende meteorite. *Astrophys. J.* **308,** L27–L30 (1986).

Acknowledgements

We thank N. S. Belshaw for assistance with mass spectrometry; A. Galy for discussions and for providing solution aliquots of some samples analysed; G. Turner and F. Albarède for comments on the manuscript; and M. Price for providing samples of the Mt and OUM series. This work was supported by the Natural Environment Research Council.

Correspondence and requests for materials should be addressed to X.K.Z. (e-mail: xiangz@earth.ox.ac.uk).

Entanglement of the orbital angular momentum states of photons

Alois Mair*, Alipasha Vaziri, Gregor Weihs & Anton Zeilinger

Institut für Experimentalphysik, Universität Wien, Boltzmanngasse 5, 1090 Wien, Austria

Entangled quantum states are not separable, regardless of the spatial separation of their components. This is a manifestation of an aspect of quantum mechanics known as quantum non-locality[1,2]. An important consequence of this is that the measurement of the state of one particle in a two-particle entangled state defines the state of the second particle instantaneously, whereas neither particle possesses its own well-defined state before the measurement. Experimental realizations of entanglement have hitherto been restricted to two-state quantum systems[3–6], involving, for example, the two orthogonal polarization states of photons. Here we demonstrate entanglement involving the spatial modes of the electromagnetic field carrying orbital angular momentum. As these modes can be used to define an infinitely dimensional discrete Hilbert space, this approach provides a practical route to entanglement that involves many orthogonal quantum states, rather than just two Multi-dimensional entangled states could be of considerable importance in the field of quantum information[7,8], enabling, for example, more efficient use of communication channels in quantum cryptography[9–11].

Multi-dimensional entanglement is a way—in addition to multi-particle entanglement—to extend the usual two-dimensional two-particle state. There have been suggestions[12,13] (and only a proof-of-principle experiment[14]) as to how to realize higher-order entanglement via multiport beam splitters. Here we present an experiment in which we used the spatial modes of the electromagnetic field carrying orbital angular momentum to create multi-dimensional entanglement. The advantage of using these modes to create entanglement is that they can be used to define an infinitely dimensional discrete (because of the quantization of angular momentum) Hilbert space.

The experimental realization proceeded in the following two steps. First, we confirmed that spontaneous parametric down-conversion conserves the orbital angular momentum of photons. This was done for pump beams carrying orbital angular momenta of $-\hbar$, 0 and $+\hbar$ per photon, respectively. Second, we showed that the state of the down-converted photons can not be explained by assuming classical correlation—in the sense that the photon pairs produced are just a mixture of the combinations allowed by conservation of angular momentum. We proved that, in contrast, they are a coherent superposition of these combinations, and hence they have to be considered as entangled in their orbital angular momentum. After completion of the experimental work presented here, related theoretical work was brought to our attention[15,16].

We will now discuss in order the two steps mentioned above. For paraxial light beams, Laguerre–gaussian (LG) modes (Fig. 1) define a possible set of basis vectors. As predicted[17] and observed[18], LG modes carry an orbital angular momentum for linearly polarized light that is distinct from the intrinsic angular momentum of photons associated with their polarizations. This external angular momentum of the photon states is the reason why they have been suggested for gearing micromachines, and it has been shown that they can be used as optical tweezers[19–21].

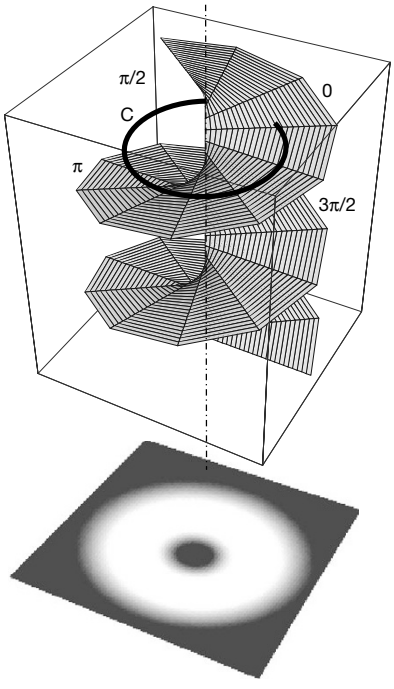

Figure 1 The wave front (top) and the intensity pattern (bottom) of the simplest Laguerre–gaussian (LG_p^l) or 'doughnut' mode. The index l is referred to as the winding number, and $(p + 1)$ is the number of radial nodes. Here we only consider cases of $p = 0$. The customary gaussian mode can be viewed as an LG mode with $l = 0$. The handedness of the helical wave fronts of the LG modes is linked to the sign of the index l, and can be chosen by convention. The azimuthal phase term $\exp il\phi$ of the LG modes results in helical wave fronts. The phase variation along a closed path C around the beam centre is $2\pi l$. Therefore, in order to fulfil the wave equation, the intensity has to vanish in the centre of the beam.

* Present address: Harvard-Smithsonian Center for Astrophysics, 60 Garden Street, Cambridge, Massachusetts 02138, USA.

To demonstrate the conservation of the orbital angular momentum carried by the LG modes in spontaneous parametric down-conversion, we investigated three different cases—for pump photons possessing orbital angular momenta of $-\hbar$, 0 and $+\hbar$ per photon, respectively. As a pump beam, we used an argon-ion laser (wavelength 351 nm) which we could operate either with a simple gaussian mode profile ($l = 0$) or in the first-order LG modes ($l = \pm 1$) after astigmatic mode conversion (for a description of this technique, see ref. 22). Spontaneous parametric down-conversion was done in a 1.5-mm-thick BBO (β-barium borate) crystal cut for type-I phase matching (that is, both photons carry the same linear polarization). The crystal cut was chosen so as to produce down-converted photons at a wavelength of 702 nm at an angle of 4° off the pump direction.

The mode detection of the down-converted photons was performed for gaussian and LG modes. The gaussian mode ($l = 0$) was identified using mono-mode fibres (Fig. 2) in connection with avalanche detectors. All other modes have a larger spatial extension, and therefore cannot be coupled into the mono-mode fibre. The LG modes ($l \neq 0$) were identified using mode detectors consisting of computer-generated holograms and mono-mode optical fibres (Fig. 2).

Computer-generated holograms have often been exploited for creating LG modes of various orders[23]. Our holograms were phase gratings 5 mm × 5 mm in size, with 20 lines mm^{-1}, which we first recorded on holographic films and bleached afterwards to increase the transmission efficiency (Fig. 2). We made holograms that had one or two dislocations in the centre, and designed them to have their maximum intensity in the first diffraction order. This enabled us to distinguish between LG modes $l = -2, -1, 0, 1, 2$ using all holograms in the first diffraction order—for which they have been blazed. For analysing an LG mode with a negative index, the holograms were rotated by 180° around the axis perpendicular to the grating lines. The total transmission efficiency of all our holograms was about 80%, and they diffracted 18% of the incoming beam into the desired first order. These characteristics were measured at 632 nm wavelength because a laser source at 702 nm was not available.

The diffraction efficiency is not the only loss that occurs. We also have to account for Fresnel losses at all optical surfaces (95% transmission), imperfect coupling into the optical fibres (70% for a gaussian beam), non-ideal interference filters (75% centre transmission), and the efficiency of the detectors (30%). A conservative estimate of all the losses yields an overall collection efficiency of 2–3%. Comparing the unnormalized ($l_{\mathrm{pump}} = l_1 = l_2 = 0$) coincidence rates of about 2,000 s^{-1} to the single count rates of about 100,000 s^{-1} we deduce an efficiency of 2%, in agreement with the above estimation.

The mode analysis was performed in coincidence for all cases where mode filter 1 was prepared for analysing LG modes $l_1 = 0, 1, 2$ and mode filter 2 for those with $l_2 = -2, -1, 0, 1, 2$. For analysing an LG mode with mode index $l = 0$—that is, a gaussian mode—the dislocation of the hologram was shifted out of the beam path. Thus the beam was sent through the border of the hologram where it acts as a conventional grating without changing the photons' angular momentum. The results are shown in Fig. 3 for different values of orbital angular momenta of the pump beam. Within experimental accuracy, coincidences were only observed in those cases where the sum of the orbital angular momenta of the down-converted photons was equal to the pump beam's orbital angular momentum. However, the absolute count rates of these cases are not equal. This is probably due to unequal emission probabilities of the photons into the different modes in the down-conversion process.

These results confirm conservation of the orbital angular momentum in parametric down-conversion. The signal-to-noise ratios achieved were as high as $V = 0.976 \pm 0.038$ and $V = 0.916 \pm 0.009$ for pump beams with and without orbital angular momentum, respectively. V is defined as $(I_{\mathrm{out}} - I_{\mathrm{in}})/(I_{\mathrm{out}} + I_{\mathrm{in}})$, where I_{in} and I_{out} denote the maximum and the minimum of the coincidences with the dislocation of the hologram respectively in and out of the beam.

It is only by using a coincidence measurement that we could show that the conservation of the orbital angular momentum holds for each single photon pair. In contrast, cumulative detection methods using many photons result in an incoherent pattern[24], because

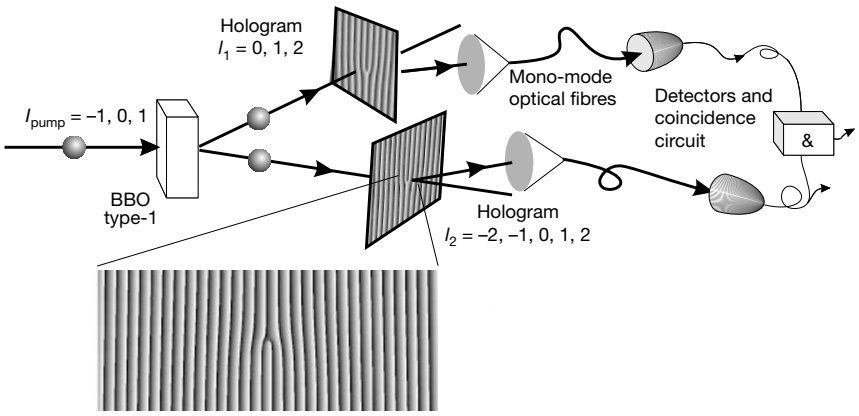

Figure 2 Experimental set-up for single-photon mode detection. After parametric down-conversion, each of the photons enters a mode detector consisting of a computer-generated hologram and a mono-mode optical fibre. By diffraction at the hologram, the incoming mode undergoes a mode transformation in such a way that an LG mode can be transformed into a gaussian mode. As it has a smaller spatial extension than all LG modes, only the gaussian mode can be coupled into the mono-mode fibre. Thus observation of a click projects the mode incident on the fibre coupler into the gaussian mode. The hologram is a phase grating with Δm dislocations in the centre blazed for first-order diffraction. An incoming gaussian laser beam passing through the dislocation of the hologram is diffracted by the grating, and the nth diffraction order becomes an LG mode with an index $l = n\Delta m$ and vice versa. Intuitively speaking, the phase dislocation exerts a 'torque' onto the diffracted beam because of the difference of the local grating vectors in the upper and lower parts of the grating. This 'torque' depends on the diffraction order n and on Δm. Consequently the right and left diffraction orders gain different handedness. Reversing this process, a photon with angular momentum $\Delta m\hbar$ before the grating can be detected by the mono-mode fibre detector placed in the first diffraction order. A photon with zero angular momentum (gaussian mode) is detected by diffracting the beam at the border of the hologram far away from the dislocation. All our measurements were performed in coincidence detection between the two down-converted photons.

each beam from parametric down-conversion by itself is an incoherent mixture. Therefore some previous workers[24] using these classical detection methods—which are in principle unsuitable at the single photon level—were led to believe that the orbital angular momentum is not conserved in spontaneous parametric down-conversion.

Given this experimental verification of the conservation of orbital angular momentum, entanglement between the two photons produced in the conversion process might be expected. But to explain the conservation of the orbital angular momentum, the photons do not necessarily have to be entangled: it would be sufficient to assume classical correlation. But further experimental results (see below) showed that the two-photon state goes beyond classical correlation, and indeed, we were able to prove the entanglement for photon states with phase singularities.

To confirm entanglement, we have to demonstrate that the two-photon state is not just a mixture but a coherent superposition of product states of the various gaussian and LG modes which obey angular momentum conservation. For simplicity, we restricted ourselves to superpositions of two basis states only. An important distinction between coherent superposition and incoherent mixture of gaussian and LG modes is that the latter possess no phase singularity. This is because adding the spatial intensity distributions of these two modes will yield a finite intensity everywhere in the resulting pattern. In contrast, in a coherent superposition the amplitudes are added, and therefore the phase singularity must remain and is displaced to an eccentric location (Fig. 4). It will appear at that location where the amplitudes of the two modes are equal, with opposite phase. Therefore the radial distance of the singularity from the beam centre is a measure of the amplitude ratio of the gaussian to the LG components, whereas the angular position of the singularity is determined by their relative phase. Intuitively speaking, the position of the dislocation with respect to the beam is equivalent to the orientation of a polarizer.

Superpositions of LG and gaussian modes can be realized experimentally by shifting the dislocation of the hologram out of the centre of the beam by a certain (small) amount. Hence in order to detect a photon having an orbital angular momentum that is a superposition of the gaussian and the LG mode, the hologram was placed in a position such that the dislocation was slightly displaced from the beam centre. In the intensity pattern these modes possess an eccentric singularity (Fig. 4). To demonstrate the entanglement, we therefore shifted one of the holograms and scanned the gaussian mode filter on the other side while recording the coincidences.

The results shown in Fig. 4 verify the correlation in superposition bases of the LG ($l = \pm 2$) and gaussian ($l = 0$) modes. A closer analysis shows that there are two conditions necessary to obtain the measured curves. First, the shifted hologram has to work as described above, and second, the source must emit an angular-momentum-entangled state. Assume that the source only emits classically correlated but not entangled singularities. Then on the side with the shifted hologram, the various terms of the classical mixture would be projected onto a state with displaced singularity leaving the total state again in a mixture. Respecting the conservation of angular momentum we would then have to sum the probabilities of the various components on the other side, resulting

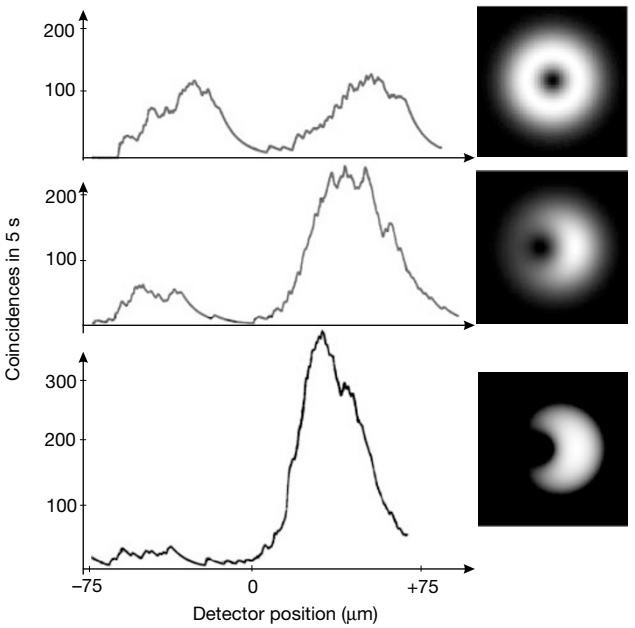

Figure 4 Experimental evidence (left; right, simulation) of entanglement of photon states with phase singularities. The dislocation of the hologram in the beam of photon 1 is shifted out of the beam centre step by step (top, middle, bottom). In these positions, this hologram—together with the mono-mode fibre detector—projects the state of photon 1 into a coherent superposition of LG and gaussian modes. The mode filter for photon 2 with the hologram taken out makes a scan of the second photon's intensity distribution (detector position) in order to identify the location of its singularity with respect to the beam centre. The coincidences show that the second photon is also detected in a superposition of LG and gaussian modes. Classical correlation would yield a coincidence picture which is just a mixture of gaussian and LG modes. In that case, the intensity minimum would remain in the beam centre but would become washed out. In the experiment a hologram with two dislocations in the first diffraction order was used.

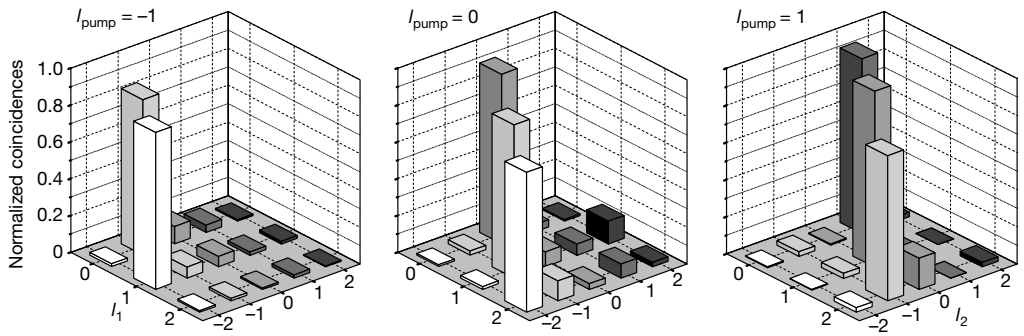

Figure 3 Conservation of orbital angular momentum. Coincidence mode detections for photon 1 and photon 2 in 15 possible combinations of orthogonal states were performed. This was done for a pump beam having an orbital angular momentum of $-\hbar$, 0 and $+\hbar$ per photon, respectively. Coincidences were observed in all cases where the sum of the orbital angular momenta of the down-converted photons was equal to the pump beam's orbital angular momentum. The coincidence counts for each fixed value of the orbital angular momentum of photon 1 were normalized by the total number of coincidences varying the orbital angular momentum of photon 2.

in a coincidence pattern not containing any intensity zeroes. Such a coincidence pattern would also be observed if a shifted hologram together with a mono-mode detector were not able to analyse for superposition states.

An entangled state represents correctly both the correlation of the eigenmodes and the correlations of their superpositions. Having experimentally confirmed the quantum superposition for $l = 0$ and $l = \pm 2$, it is reasonable to expect the quantum superposition will also occur for the other states. Nevertheless, ultimate confirmation of entanglement will be a Bell inequality experiment generalized to more states[25]. Such an experiment will be a major experimental challenge, and we are preparing to perform it.

For a pump beam with zero angular momentum, the emitted state must then be represented by

$$\psi = C_{0,0}|0\rangle|0\rangle + C_{1,-1}|1\rangle|-1\rangle + C_{-1,1}|-1\rangle|1\rangle + C_{2,-2}|2\rangle|-2\rangle + C_{-2,2}|-2\rangle|2\rangle + \ldots\ldots \quad (1)$$

as the LG modes form an infinite dimensional basis. Here the numbers in the brackets represent the indices l of the LG modes, and the $C_{i,j}$ denote the corresponding probability amplitude for measuring $|i\rangle|j\rangle$. The state (1) is a multi-dimensional entangled state for two photons, which in general will also contain terms with radial mode index $p \neq 0$. It means neither photon in state (1) possesses a well-defined orbital angular momentum after parametric down-conversion. The measurement of one photon defines its orbital angular momentum state, and projects the second one into the corresponding orbital angular momentum state.

It is conceivable that these states could in the future be extended to multi-dimensional multi-particle entanglement. A growing body of theoretical work calls for entanglement of quantum systems of higher dimensions[7,8]. These states have applications in quantum cryptography with higher alphabets and in quantum teleportation. As such states increase the flux of information, it is conceivable that they could be important for many other applications in quantum communication and in quantum information. The possibility of using these photon states to drive micromachines, and the application of these states as optical tweezers, make them versatile and potentially suitable for future technologies[19–21]. □

Received 12 March; accepted 5 June 2001.

1. Schrödinger, E. Die gegenwärtige Situation in der Quantenmechanik. *Naturwissenschaften* **23,** 807–812; 823–828; 844–849 (1935).
2. Schrödinger, E. Discussion of probability relations between separated systems. *Proc. Camb. Phil. Soc.* **31,** 555–563 (1935).
3. Bouwmeester, D., Pan, J.-W., Daniell, M., Weinfurter, H. & Zeilinger, A. Observation of a three-photon Greenberger-Horne-Zeilinger state. *Phys. Rev. Lett.* **82,** 1345–1349 (1999).
4. Pan, J.-W., Bouwmeester, D., Daniell, M., Weinfurter, H. & Zeilinger, A. Experimental test of quantum nonlocality in three-photon Greenberger-Horne-Zeilinger entanglement. *Nature* **403,** 515–519 (2000).
5. Sackett, C. A. *et al*. Experimental entanglement of four particles. *Nature* **404,** 256–259 (2000).
6. Pan, J.-W., Daniell, M., Gasparoni, S., Weihs, G. & Zeilinger, A. Experimental demonstration of four-photon entanglement and high-fidelity teleportation. *Phys. Rev. Lett.* **86,** 4435–4438 (2001).
7. DiVincenzo, D. P., More, T., Shor, P. W., Smolin, J. A. & Terhal, B. M. Unextendible product bases, uncompletable product bases and bound entanglement. Preprint quant-ph/9908070 at ⟨http://xxx.lanl.gov⟩ (1999).
8. Bartlett, S. D., de Guise, H. & Sanders, B. C. Quantum computation with harmonic oscillators. Preprint quant-ph/0011080 at ⟨http://xxx.lanl.gov⟩ (2000).
9. Bechmann-Pasquinucci, H. & Peres, A. Quantum cryptography with 3-state systems. *Phys. Rev. Lett.* **85,** 3313–3316 (2000).
10. Bechmann-Pasquinucci, H. & Tittel, W. Quantum cryptography using larger alphabets. *Phys. Rev. A* **61,** 62308–62313 (2000).
11. Bourennane, M., Karlsson, A. & Björk, G. Quantum key distribution using multilevel encoding. *Phys. Rev. A* (in the press).
12. Reck, M., Zeilinger, A., Bernstein, H. J. & Bertani, P. Experimental realization of any discrete unitary operator. *Phys. Rev. Lett.* **73,** 58–61 (1994).
13. Zukowski, M., Zeilinger, A. & Horne, M. Realizable higher-dimensional two-particle entanglements via multiport beam splitters. *Phys. Rev. A* **55,** 2564–2579 (1997).
14. Reck, M. *Quantum Interferometry with Multiports: Entangled Photons in Optical Fibers.* Thesis, Univ. Innsbruck (1996).
15. Arnaut, H. H. & Barbosa, G. A. Orbital and angular momentum of single photons and entangled pairs of photons generated by parametric down-conversion. *Phys. Rev. Lett.* **85,** 286–289 (2000).
16. Franke-Arnold, S., Barnett, S. M., Padgett, M. J. & Allen, L. Two-photon entanglement of orbital angular momentum states. *Phys. Rev. A* (in the press).
17. Allen, L., Beijersbergen, M. W., Spreeuw, R. J. C. & Woerdman, J. P. Orbital angular momentum of light and the transformation of laguerre-gaussian laser modes. *Phys. Rev. A* **45,** 8185–8189 (1992).
18. He, H., Fries, M., Heckenberg, N. & Rubinsztein-Dunlop, H. Direct observation of transfer of angular momentum to absorbtive particles from a laser beam with a phase singularity. *Phys. Rev. Lett.* **75,** 826–829 (1995).
19. Simpson, N. B., Dholakia, K., Allen, L. & Padgett, M. J. Mechanical equivalence of spin and orbital angular momentum of light: An optical spanner. *Opt. Lett.* **22,** 52–54 (1997).
20. Galajda, P. & Ormos, P. Complex micromachines produced and driven by light. *Appl. Phys. Lett.* **78,** 249–251 (2001).
21. Friese, M. E. J., Enger, J., Rubinsztein-Dunlop, H. & Heckenberg, N. Optical angular-momentum transfer to trapped absorbing particles. *Phys. Rev. A* **54,** 1593–1596 (1996).
22. Bejersbergen, M. W., Allen, L., van der Veen, H. E. L. O. & Woerdman, J. P. Astigmatic laser mode converters and transfer of orbital angular momentum. *Opt. Commun.* **96,** 123–132 (1993).
23. Arlt, J., Dholakia, K., Allen, L. & Padgett, M. J. The production of multiringed laguerre-gaussian modes by computer-generated holograms. *J. Mod. Opt.* **45,** 1231–1237 (1998).
24. Arlt, J., Dholakia, K., Allen, L. & Padgett, M. Parametric down-conversion for light beams possessing orbital angular momentum. *Phys. Rev. A* **59,** 3950–3952 (1999).
25. Kaszlikowski, D., Gnacinski, P., Zukowski, M., Miklaszewski, W. & Zeilinger, A. Violation of local realism by two entangled n-dimensional systems are stronger than for two qubits. *Phys. Rev. Lett.* **85,** 4418–4421 (2000).

Acknowledgements

This work was supported by the Austrian Fonds zur Förderung der wissenschaftlichen Forschung (FWF).

Correspondence and requests for materials should be addressed to A.Z. (e-mail: anton.zeilinger@univie.ac.at).

Superconductivity in the non-magnetic state of iron under pressure

Katsuya Shimizu*†, Tomohiro Kimura*, Shigeyuki Furomoto*, Keiki Takeda*, Kazuyoshi Kontani*, Yoshichika Onuki‡ & Kiichi Amaya*†

** Department of Physical Science, Graduate School of Engineering Science, Osaka University, Toyonaka, Osaka 560-8531, USA*
† Research Center for Materials Science at Extreme Conditions, Osaka University, Toyonaka, Osaka 560-8531, Japan
‡ Department of Physics, Graduate School of Science, Osaka University, Osaka 560-0043, Japan

Ferromagnetism and superconductivity are thought to compete in conventional superconductors, although in principle it is possible for any metal to become a superconductor in its non-magnetic state at a sufficiently low temperature. At pressures above 10 GPa, iron is known to transform to a non-magnetic structure[1,2] and the possibility of superconductivity in this state has been predicted[3,4]. Here we report that iron does indeed become superconducting at temperatures below 2 K at pressures between 15 and 30 GPa. The transition to the superconducting state is confirmed by both a drop in resistivity and observation of the Meissner effect.

An iron sample with purity of 99.995% (Johnson Matthey) was purified further and degassed by heating close to the melting point in an ultra-high-vacuum chamber. The sample was cut into a rectangular shape of $0.04 \times 0.160 \times 0.07\,\mathrm{mm}^3$ and placed in the sample chamber of a non-magnetic diamond-anvil cell (DAC) made of BeCu alloy. For electrical resistivity measurements the BeCu metal gasket was covered with a thin Al_2O_3 layer for electrical insulation. Electrical resistivity measurements are performed using the a.c. four-terminal method with a typical measuring current of 0.1×10^{-6} A at low temperatures below 10 K. The sample chamber was filled with NaCl as the pressure-transmitting medium (Fig. 1a). Several ruby chips of less than 0.002 mm in diameter were located around the sample and the applied pressure